REMOTE SENS. ENVIRON. 35:201–211 (1991)

Surface Albedo from Bidirectional Reflectance

K. J. Ranson and J. R. Irons

Biospheric Sciences Branch, NASA Goddard Space Flight Center, Greenbelt, Maryland

C. S. T. Daughtry

Remote Sensing Research Laboratory, USDA Agricultural Research Service, Beltsville, Maryland

Total hemispherical shortwave reflectance (albedo) is a major parameter of interest for studies of land surface climatology and global change. Efforts to estimate albedo from remote sensing data have been constrained by the available instrumentation that typically provide observations of reflected radiance from a single view direction in narrow spectral bands. However, the capability to obtain multiple angle observations over the shortwave region is planned for Earth Observing System sensors. In this paper, methods for estimating albedo from multiple angle, discrete wavelength band radiometer measurements are examined. The methods include a numerical integration technique and the integration of an empirically derived equation for bidirectional reflectance. The validity of the described techniques is examined by comparing albedo computed from multiband radiometer data with simultaneously acquired pyranometer data from vegetated and bare soil surfaces. Shortwave albedo estimated from both techniques agree favorably with the independent pyranometer measurements. Absolute root mean square errors were 0.5% or less for both grass sod and bare soil surfaces.

INTRODUCTION

As a component of the radiation budget, total hemispherical shortwave reflectance (albedo) is a major parameter of interest to biospheric (e.g., Sellers, 1985) and climatological (e.g., Dickinson, 1983) studies. In addition, surface albedos are required for radiative transfer models, numerical weather prediction models, and global climate models (Wiesnet and Matson, 1983). Past efforts to estimate albedo from remote sensing data have been constrained by the available instrumentation (Pinker and Ewing, 1986). Since albedo is the total reflectance of the surface integrated over all angles of the upward hemisphere, it cannot be directly measured by aircraft- or spacecraft-based remote sensing instrumentation. As a consequence, albedo is often assumed invariant with land surface cover (Pinker and Stowe, 1990; Saunders, 1990) or assumed to be equivalent to nadir reflectance factor.

Over the past decade numerous studies have been conducted to estimate albedo or spectral hemispherical reflectance of surfaces from bidirec-

Address correspondence to Jon Ranson, NASA/Goddard Space Flight Center, Code 923, Greenbelt, MD 20771.

Received June 1990; revised 12 November 1990.

0034-4257/91/$3.50
Published 1991 by Elsevier Science Publishing Co. Inc., 655 Avenue of the Americas, New York, NY 10010

tional reflectance measurements. Kriebel (1979) calculated the total shortwave albedo of four cover types (savannah, bog, pasture land, and coniferous forest) from multiple direction data obtained by an airborne, eight channel, scanning radiometer. Kimes and Sellers (1985) computed spectral hemispherical reflectances of several bare fields, grass canopies, and row crop canopies from multiple direction observations obtained with a field radiometer. Walthall et al. (1985) developed a three-term equation which describes bidirectional reflectance as a function of view direction relative to the solar direction. The equation was fit to multiple direction data from several bare soil surfaces and a soybean canopy. The equation was then analytically integrated to derive hemispherical reflectances for the various surfaces. Irons et al. (1987) used the equation of Walthall et al. (1985) to estimate the spectral hemispherical reflectances of bare soil, soybeans, and orchardgrass from multiple direction data acquired by a pointable, airborne, imaging radiometer.

Several researchers have examined the errors involved in estimating hemispherical reflectance from nadir or off-nadir reflectance measurements. The study of Kimes and Sellers (1985) showed errors as great as 45% when they compared estimates of hemispherical reflectance derived from nadir measurements to estimates derived from a series of off-nadir measurements. Kimes et al. (1987) continued the analysis of hemispherical reflectance to include multiple nadir spectral reflectances and multiple off-nadir view angles acquired in specific azimuthal planes. Hemispherical reflectances inferred from nadir observations were reported to be in error by as much as 26%, whereas utilizing several off-nadir measurements within a given azimuth direction improved the error to 4%. Irons et al. (1988) expanded the methods reported by Kimes to include integration over seven discrete wavelength bands within the 0.4–2.4 μm portion of the spectrum. They used these techniques to follow the diurnal and seasonal dynamics of shortwave albedo of prairie grass. In all of the above studies "true" values of hemispherical spectral reflectance or shortwave albedo were derived from the full set of off-nadir measurements and not from independent data from a hemispherical sensor such as a pyranometer.

In the study reported here the validity of integrating over discrete wavelength bands to estimate total shortwave bidirectional reflectance of vegetated and bare soil surfaces is examined. In addition, the angular integration techniques reported by Kimes and Sellers (1985) and the empirical model approach of Walthall et al. (1985) for estimating hemispherical reflectance were evaluated using independent shortwave albedo data (i.e., pyranometer data) acquired coincident with bidirectional reflectance measurements of grass and bare soil surfaces.

Table 1. Downwelling Solar Irradiance at the Earth's Surface as a Function of Spectral Band[a]

i	*Spectral Band (μm)*	*Corresponding MMR Spectral Band (μm)*	*Total Downwelling Irradiance (W/m^2)*
1	0.30–0.52	0.45–0.52	110
2	0.52–0.62	0.52–0.62	100
3	0.62–0.69	0.63–0.69	63
4	0.69–1.15	0.75–0.88	255
5	1.15–1.35	1.15–1.30	60
6	1.35–1.50	—	4
7	1.50–1.85	1.50–1.85	51
8	1.85–2.08	—	6
9	2.08–2.35	2.08–2.35	19
10	2.35–3.00	—	3

[a]Values derived from the LOWTRAN-6 computer code (Kneizys et al., 1983) for a clear, rural midlatitude atmosphere with solar zenith angle = 45°.

DATA ACQUISITION

A Barnes Model 12-1000 Modular Multiband Radiometer (MMR) with a 15° field-of-view (FOV) was used to measure reflected radiance in seven spectral bands (Table 1) from fields of bluegrass sod (*Poa sp.*) and bare soil (fine-loamy, mixed, mesic Fluvaquentic Dystrochrept). The grass field was uniform, level, and mowed to a height of 5 cm before data acquisition. The bare soil field was also level with a moderately rough surface produced by tilling with a disk plow (Irons and Smith, 1990).

The radiometer was mounted on a boom at 2.0 m above the soil surface and reflected radiance was measured sequentially at 15 view zenith angles (out to 70° on both sides of nadir in 10° increments) in each of four azimuthal planes for a total of 60 observations. Operationally, the instrument was aligned with the solar principal plane by positioning the shadow cast by a thin dowel along the axis of the boom. Rotating the boom 90° aligned

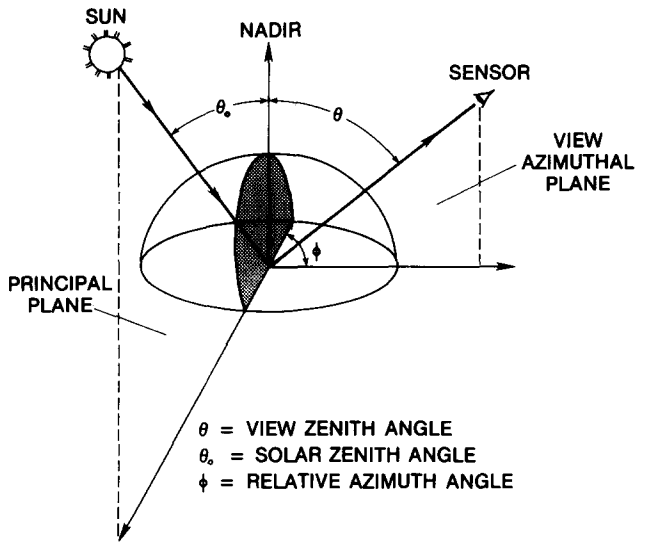

Figure 1. Geometry of bidirectional reflectance measurements: θ = view zenith angle; θ_0 = solar zenith angle; ϕ = azimuth angle relative to the solar principal plane.

the instrument with the principal plane. The measurement sequence was started with the instrument pointed in the direction of the sun at a view zenith angle of 70° and continued at 10° increments through nadir and out to 70° in the antisolar direction. The boom was rotated 45° in azimuth and measurements were acquired for azimuth directions of 45° and 225°. This procedure was repeated by rotating the boom in increments of 45° to acquire view zenith measurements for azimuths of 90° and 270°, and 135° and 315° thus completing a set of 60 angular measurements. By continuing in a clockwise direction, a second set of observations were similarly acquired. With this method it was possible to acquire the two full sets of 60 angles in less than 10 min.

The geometry of these observations is illustrated in Figure 1. Note that the azimuthal plane of observation is defined by the sensor, the target, and a line through the target perpendicular to the surface. The principal azimuthal plane is defined by the sun, the target, and the perpendicular line through the target.

A second MMR was positioned over a barium sulfate ($BaSO_4$) painted panel and spectral radiances were measured at 30-s intervals throughout the day. In addition, a pair of Eppley pyranometers were mounted on a boom with one measuring hemispherical downwelling shortwave (0.3–2.8 μm) radiation (pointing skyward) and the other measuring hemispherical reflected radiance from

Table 2. Data Acquisition Times and Solar Angle Limits for Bidirectional Reflectance Measurements

Date (Target)	*Data Set Number*	*Time (EDT)*		*Solar Zenith Angle (deg)*		*Solar Azimuth Angle (deg)*	
		Start	*End*	*Start*	*End*	*Start*	*End*
5/12/1988	1	1009	1019	43	41	108	108
(sod)	2	1030	1043	39	37	110	114
	3	1100	1111	34	32	118	122
	4	1132	1142	29	27	129	133
	5	1200	1210	25	24	141	146
	6	1228	1239	22	21	156	163
	7	1303	1313	21	21	180	185
	8	1330	1339	21	22	196	202
	9	1403	1418	24	26	215	222
	10	1426	1435	27	28	226	230
	11	1500	1510	32	34	238	242
	12	1531	1541	38	39	247	250
	13	1559	1608	43	44	254	256
	14	1631	1647	49	52	260	263
	15	1700	1709	54	56	265	267
	16	1735	1744	61	63	271	272
	17	1758	1808	66	68	275	276
	18	1830	1839	72	74	279	281
6/29/1989							
(bare soil)	1	1626	1636	44	46	264	266
	2	1704	1714	51	53	270	272
	3	1830	1838	68	70	283	284
	4	1907	1915	75	76	288	289
6/30/1989							
(bare soil)	1	912	921	53	51	89	90
	2	946	955	46	44	94	96
	3	1042	1050	35	34	105	107
	4	1138	1147	25	24	122	125
	5	1423	1435	22	24	229	235
	6	1522	1531	32	34	250	252
	7	1611	1619	41	43	261	263
	8	1643	1652	47	48	267	268
	9	1653	1700	49	51	268	269

the surface. Upward and downward pyranometer measurements were collected at 30-s intervals while the experiments were in progress. Prior to the field studies the MMRs and pyranometers were calibrated to ensure consistent results between like instruments.

Reflectance factor and shortwave albedo data were acquired for the grass on 15 May 1988, and for the bare soil surface on 29 and 30 June 1989, at several times during each day. All three days were essentially cloud free with low observable haze. Table 2 lists the time of day and solar zenith and azimuth angles for each analyzed data set.

Under certain sun-view angle conditions the instrument and/or supporting apparatus cast a shadow in the FOV. Such observations were removed from the data sets. In each spectral band,

replicated observations for a view direction were averaged and these average spectral bidirectional reflectance factors were used in the computation of albedo as discussed below.

COMPUTATIONAL METHODS

Spectral reflectance factors were derived from ratios of the spectral radiance reflected from the surfaces to the spectral radiance reflected from the barium sulfate painted reference panel by

$$R(\theta,\phi,\theta_0;\lambda)=\frac{L(\theta,\phi;\theta_0;\lambda)}{L_{\text{ref}}(\theta_0,\lambda)}R_{\text{ref}}(\theta_0,\lambda). \quad (1)$$

$R(\theta,\phi;\theta_0;\lambda)$ is a surface bidirectional reflectance factor measured at view zenith angle θ, solar zenith angle θ_0, view azimuth angle ϕ, in spectral band λ. $L(\theta,\phi;\theta_0;\lambda)$ and $L_{\text{ref}}(\theta_0,\lambda)$ are the observed surface and $BaSO_4$ panel radiances, respectively. The measured bidirectional reflectance factor of the reference panel (measured *a priori* in the laboratory), $R_{\text{ref}}(\theta_0,\lambda)$ corrects for nonideal (i.e., not perfectly reflecting, Lambertian) reflectance characteristics of the panel (Robinson and Biehl, 1979). By definition, the use of the term bidirectional indicates the measurement of directional radiation in infinitesimally small, and impractical to measure, solid angles. However, according to Robinson and Biehl (1979), Eq. (1) can be used to approximate bidirectional reflectance factors if the conditions of view and illumination are the same for the target and reference surface, the bidirectional reflectance properties of the reference surface are known, the FOV of the instrument is sufficiently small ($< 20°$), and the incident radiation is dominated by the directional component.

Albedo is the ratio of total shortwave (0.30–3.00 μm) radiation flux reflected by a surface in all directions within the surrounding 2π steradian solid angle (i.e., hemisphere) to the total downwelling solar flux. Estimation of albedo from the spectral bidirectional reflectance factors calculated by Eq. (1) was accomplished by two numerical integrations of the data.

The numerical integration used to derive bidirectional reflectance factors over the shortwave region was essentially an average of reflectance factors in 10 spectral bands weighted by the downwelling solar flux in each of the bands (Irons et al., 1988). Kriebel (1979) used a similar weighted average of spectral reflectances in his calculations of albedos for several vegetated surfaces. Jackson (1984) has also calculated the total reflected solar radiation from multispectral MMR data using an alternative computational approach. In the approach used here shortwave bidirectional reflectance factors (ρ) were computed as

$$\rho=\int_{0.3}^{3.0}R(\lambda)E(\lambda)d(\lambda)\Big/\int_{0.3}^{3.0}E(\lambda)d(\lambda), \quad (2)$$

$$\rho\simeq\sum_{i=1}^{10}R_iE_i\Delta\lambda_i\Big/\sum_{i=1}^{10}E_i\Delta\lambda_i, \quad (3)$$

where λ indicates wavelength, $\Delta\lambda_i$ represents a spectral band width, E_i represents downwelling spectral irradiance in band i, and R_i represents a spectral reflectance factor at a particular view direction in band i.

The shortwave region was broken into 10 spectral bands as suggested by Irons et al. (1988) for the purpose of numerical integration. The LOWTRAN 6 computer code for atmospheric transmittance (Kneizys et al., 1983) was used to generate downwelling solar flux densities in the 10 spectral bands (Table 1). A clear rural atmosphere (23 km visibility) typical of a midlatitude region in the summer was assumed for the flux calculations. Irons et al. (1988) utilized solar densities computed for a range of sun angles, since the spectral distribution of sunlight may change as a function of optical path length. We found, however, that the LOWTRAN calculations tended to overestimate changes in the spectral distribution measured during the time of the experiment, especially at larger solar zenith angles. Consequently, solar flux densities computed for a solar zenith angle of 45° were used for all shortwave bidirectional reflectance calculations. Figure 2 presents comparisons of the proportions of in-band spectral irradiances in each MMR band measured at three solar zenith angles (21°, 45°, 70°) and those computed using LOWTRAN 6 (45° only). The curves agree well for all wavelength bands except for 0.42–0.52 μm. The differences in measured and LOWTRAN calculated in-band irradiance proportions are caused by a larger diffuse irradiance component in the measured irradiances. The solar flux densities used in Eq. (3) are listed in Table 1.

Reflectance factors in three spectral regions not covered by the MMR (1.30–1.50 μm,

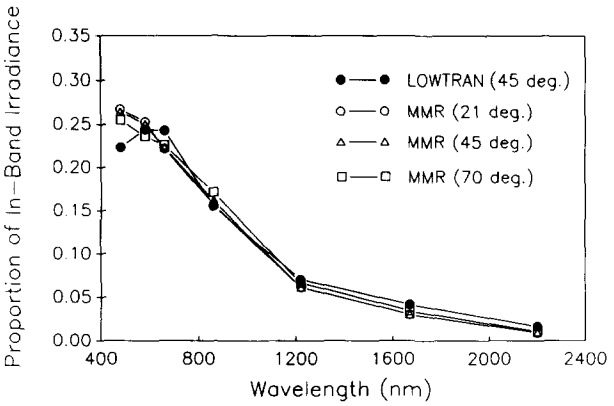

Figure 2. Comparison of in-band spectral irradiances measured at three solar zenith angles (21°, 45°, 70°) and those computed using LOWTRAN 6 (45° only).

1.80–2.08 μm, and 2.35–3.00 μm) were treated as negligible on the basis of *a priori* knowledge of typical *in situ* vegetation reflectance spectra and the small proportion of spectral irradiance in these bands (Table 1). Reflectance factors in the other seven bands were estimated from the measured reflectance factors in the MMR spectral bands. Consideration of typical vegetation reflectance spectra (Irons et al., 1988) indicated that reflectances in the MMR spectral bands were representative of reflectances in the broader spectral bands used for numerical integration (Table 1).

The second step required to calculate albedos was an integration of bidirectional reflectance factors over a 2π sr solid angle (i.e., a hemisphere). As shown by Kimes and Sellers (1985), albedo is related to a distribution of bidirectional reflectance factors by the following double integral:

$$\alpha = \pi^{-1} \int_{2\pi} \int_{\pi/2} \rho(\theta, \phi) \cos\theta \sin\theta \, d\theta \, d\phi, \quad (4)$$

where α equals albedo, $\rho(\theta, \phi)$ is a distribution of bidirectional reflectance factors at a constant solar zenith angle, θ is the view zenith angle, and ϕ is the relative azimuth angle between the solar principal plane and the view azimuthal plane. To estimate α from the available bidirectional reflectance factors, the following numerical integration was performed:

$$\alpha \simeq \pi^{-1} \sum_{j=1}^{8} \rho_j \Delta\Omega_j, \quad (5)$$

where $\Delta\Omega_j$ equals the projected solid angle of a partition of the 2π sr angle:

$$\Delta\Omega_j = \pi\left(\sin^2\theta_j - \sin^2\theta_{j-1}\right), \quad (6)$$

where $\theta_j = 0°, 5°, 15°, 25°, 35°, 45°, 55°, 65°, 90°$, for $j = 0, 1, \ldots, 8$. Each partition is represented by an annular ring in the two dimensional projection of the 2π sr solid angle [see Irons et al. (1988) for further detail]. Also, in Eq. (5), each projected solid angle is multiplied by the average of the bidirectional reflectance factor measurements made within the solid angle (i.e., the average of the eight reflectance factors corresponding to the eight view azimuth directions for a given view zenith angle):

$$\bar{\rho}_j = \sum_{k=1}^{m} \rho(\theta_j^*, \phi_k)/m, \quad \text{where } \theta_{j-1} < \theta_j^* < \theta_j. \quad (7)$$

The product of $\bar{\rho}_j$ and $\Delta\Omega_j$ is then summed over the eight solid angles to compute albedo.

The albedos were derived using all of the available bidirectional reflectance factor data. Since measurements were made in four azimuthal planes, a total of eight reflectance values ($m = 8$) were used in Eq. (7) for each solid angle except the innermost (i.e., $\Delta\Omega_1$) when an average of four nadir measurements was used.

A second approach to calculating albedo involved fitting an empirical equation suggested by Walthall et al. (1985) to the distributions of shortwave bidirectional reflectance factors derived for both the sod and the bare soil surfaces. Although the equation does not explicitly include biological or physical parameters which characterize a canopy or soil surface, Walthall reported that the equation closely reproduced measured distributions of bidirectional reflectance factors from several plant canopies and soil surfaces. The equation expresses reflectance factors as a function of illumination and viewing geometry and three empirical coefficients, a, b, and c:

$$R(\theta, \phi) = a\theta^2 - b\theta\cos(\phi) + c, \quad (8)$$

where $R(\theta, \phi)$ is percent reflectance factor, θ is the view zenith angle, and ϕ is the view azimuth angle relative to the solar principal plane. The equation describes the distribution of bidirectional reflectance factors for a constant solar zenith angle and the coefficients (a, b, and c) are dependent on solar zenith angle. The coefficients were de-

rived for the sod and bare soil surfaces by fitting Eq. (8) to the distribution of bidirectional reflectances measured for each data set using multiple linear regression (Table 2). The standard error of bidirectional reflectance factor estimates was typically about 1% with a range from 0.8% to 2.3% for Eq. (8) fit to the grass sod data. For Eq. (8) fit to bare soil data, standard errors of the estimates were usually between 2% and 3%, with a range of 1.6–5.3%.

Equation (8) can be analytically integrated over the 2π sr solid angle containing all view directions to derive an expression for albedo. The result of the integration is provided by Walthall et al. (1985) as

$$A = (2.305a/\pi) + c, \qquad (9)$$

where A is percent albedo and where the view zenith angles were expressed in radians in Eq. (8). Given the empirical coefficients a and c from Eq. (8), albedos were calculated for sod and bare soil using Eq. (9).

RESULTS AND DISCUSSION

Despite several studies indicating the non-Lambertian behavior of terrestrial surfaces, it is common practice to assume that the nadir reflectance factor approximates hemispherical spectral albedo. Although it may be practical for studies of large scale phenomena (e.g., Pinker and Stowe, 1990) or required in the absence of measurements (Saunders, 1990), the implication of assuming Lambertian behavior for estimating albedo is evident in Figure 3. Measured albedos and nadir shortwave reflectance factors calculated by Eq. (3) are compared for the grass and soil data sets in Figure 3a and b, respectively. Measured albedos plotted in Figure 3 represent the average of data collected within the time interval for the corresponding bidirectional reflectance factor data (viz., Table 2). For the grass, the nadir reflectance factor agrees with albedo within 10% at small solar zenith angles (i.e., $< 30°$). Nadir reflectance factor remains fairly constant over the range of observed sun angles whereas albedo increases with the absolute differences increasing to 37% at 73°. For the soil data, nadir reflectance factors decrease as solar zenith increases while albedo increased only slightly. Differences of over 25% occur at small sun angles and were smallest within the 45–52° range of solar zenith angles. The magnitudes and trends of these differences are consistent with those reported by Kimes and Sellars (1985), comparing hemispherical and nadir spectral reflectances of grass and bare soil surfaces.

Examination of the angular distributions of the full range of bidirectional reflectance factors is instructive for determining the sources of the discrepancies noted above. Plate IV presents plots of contours of equal reflectance factors combined with surface response plots for grass and soil bidirectional reflectance factor data acquired at different solar zenith angles. View directions are represented by polar coordinates as illustrated in Figure 4. For example, nadir is located at the origin, $(\theta, \phi) = (0°, 0°)$, and $(\theta, \phi) = (70°, 180°)$ is located at the far right of each plot. The reflectance factors distributions for grass sod at 21° (Plate IVa) varies only from 19% in the forward scatter direction [e.g., $(\theta, \phi) = (20°, 0°)$] to about 23% in the backscatter direction $(\theta, \phi) \simeq (20°, 180°)$. For the 45° solar zenith angle case (Plate IVb) the reflectance

Figure 3. Comparison of measured albedos and nadir shortwave reflectance factor for the grass (A) and soil (B) data sets.

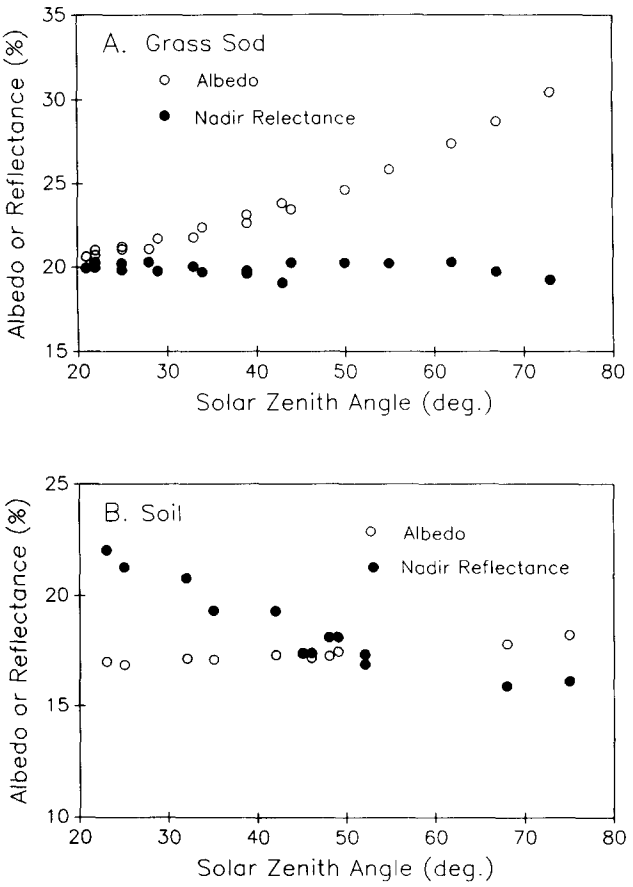

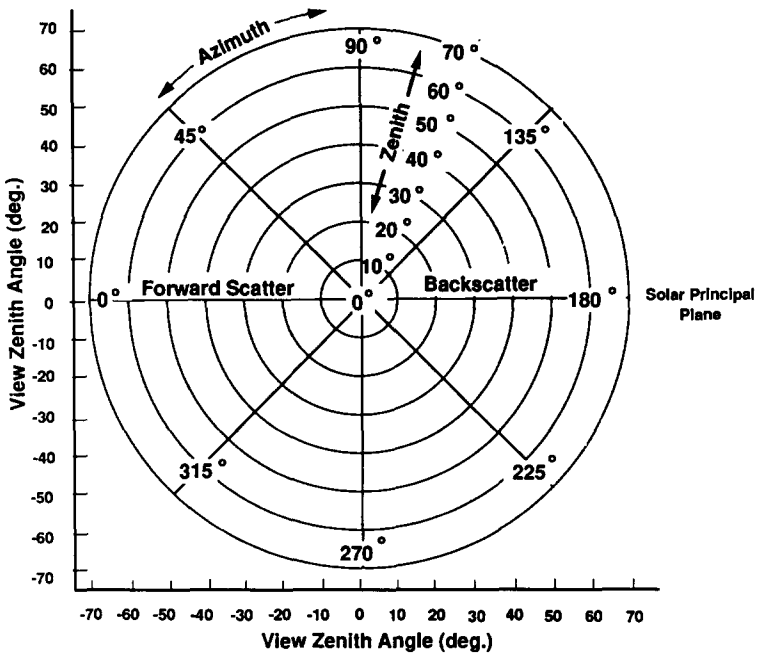

Figure 4. Polar plot showing coordinate system used to display bidirectional reflectance factor data in Plate IV.

distribution is lowest near nadir and greatest near the hot spot direction of $(\theta, \phi) = (70°, 180°)$. Reflectance factors also increase from small view zenith angles to large view zenith angles giving the distribution a bowl-like appearance. At a solar zenith angle of 67° reflectance factors increase greatly from a minimum near nadir as view zenith angle increases for all view azimuth directions. Again, the greatest increase in reflectance occurs in the backscatter direction. The reflectance behavior noted is caused by the erectophile structure of the grass leaves (i.e., mostly vertical arrangement). When viewed at near nadir angles, the FOV contains more shadows cast by the leaves and reflectance factors are relatively low. At larger view zenith angles the FOV is dominated by the reflected light from the erect grass leaves and reflectance increases [see Kimes (1983) for more details regarding directional reflectance of vegetated and bare soil surfaces, respectively]. Consequently, albedo will be weighted by this strong anisotropy, whereas nadir reflectance will vary only slightly with changing solar angle.

The soil data shortwave reflectance factor distributions for solar zenith angles of 22°, 41°, and 67° are presented in Plates IVd, IVe, and IVf, respectively. In each case reflectance factors are lowest in the forward scattering direction and increase through nadir until a maximum is reached in the backscatter direction. This is related to the relatively rough surface of the soil. For view directions in the forward scatter direction (i.e., $\phi = 0°$) the sensor FOV contains shadows cast by clods on the soil surface. When viewed from the backscatter direction (i.e., $\phi = 180°$), sunlit soil dominates the field of view. Since the proportion of the FOV containing shadows increases with larger solar zenith angles the nadir reflectance factors will decrease as the solar zenith angle increases as observed in Figure 3b. Since albedo is an integration of reflectance over all angles the strong preferential scattering observed in Plate IVe and IVf does not appear to dominate the hemispherical reflectance.

The general trends of measured albedo over the grass and soil are shown in Figures 5a and 5b, respectively. Albedos derived from upward and downward looking pyranometers at 30-s intervals are plotted against time of day and solar zenith angle. Estimates of albedo calculated with Eq. (5) with numerical integration of bidirectional reflectance factors and albedos estimated with the empirical formulation of Walthall et al. (1985) [Eq. (9)] are also shown. For the grass (Figure 5A), albedos appear to be symmetric about solar noon. Albedos were lowest at solar noon and increased by nearly 48% from noon to late afternoon. Albedos estimated with both techniques follow closely

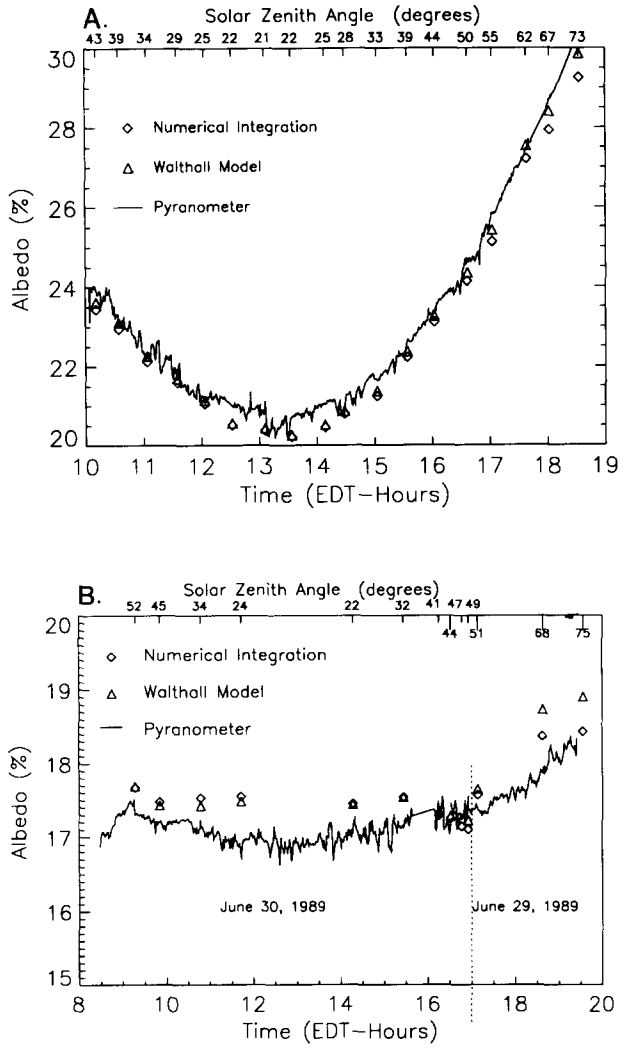

Figure 5. Diurnal trends of albedo derived from pyranometer data, numerical integration, and integrated empirical fit to the data (Walthall et al., 1985) for grass sod (A) and bare soil (B).

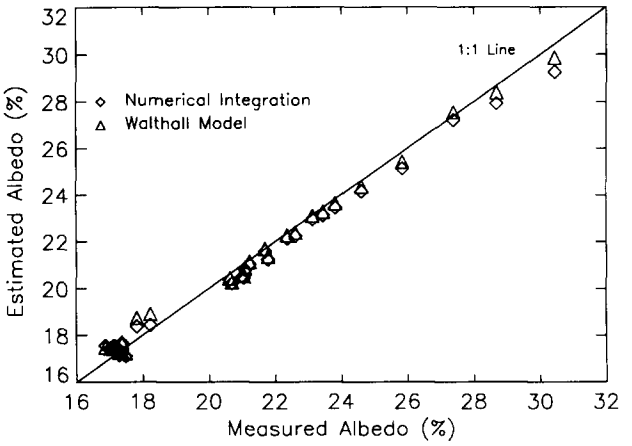

Figure 6. Estimated albedos from both the grass and bare soil plotted against pyranometer values averaged over the time interval corresponding to each bidirectional reflectance factor data set (Table 2).

the measured trend but underestimate the average of measurements with maximum relative errors of 3.8% and 2.7% for numerical integration and Walthall's model, respectively (Table 3). The albedos obtained for the bare soil (Figure 5B) also increase for sun angles away from solar noon; the changes from morning to noon or noon to afternoon are much less (< 7%) than those for the grass. Estimated albedos were greater than average measured values by as much as 4.0% (relative) using the numerical integration technique and 5.1% (relative) using the empirical model (Table 3).

To further illustrate the comparison of the two albedo estimation techniques with measurements, Figure 6 presents estimated albedos from both the grass and bare soil plotted against measured values. Measured values represent pyranometer values averaged over the time span required to acquire each set of bidirectional reflectance factor data (approximately 10 min). Regression analyses for estimated versus measured albedos were performed with the grass sod and soil data sets separately, as well as combined. In addition, two figures of merit were used to examine the errors of the two techniques. The absolute root mean square error [rmse(a)] gives the expected error with respect to the full scale of measurement (i.e., 0–100%) whereas the relative root mean square error [rmse(r)] indicates the expected error relative to measured values (Table 4).

The results of the statistical analyses are shown in Table 4. Examining the surface types separately shows that rmse(a) and rmse(r) values were about 0.5% and 2.0%, respectively, for the grass sod using the numerical integration technique. The errors improved to 0.3% and 1.3%, respectively, using the empirical model fit to the data. The results for the soil data show lower r^2, but small (< 0.5%) rmse(a) values for both techniques. The rmse(r) values for the soil were the largest found for either surface, but still less than 2.5%.

Performing similar regression analysis with the combined data sets yielded correlation coefficients (r^2) of 0.99 for both the numerical integration and empirical model techniques, respectively. Intercept (b_0) and slope (b_1) coefficients, however,

Table 3. Comparison of Albedo Estimated by Numerical Integration of BRDF, Walthall Empirical Model, and Average of Pyranometer Albedos Measured During Time of Reflectance Factor Measurements

Date	*Time EDT*	*Solar Zenith Angle (deg)*	*Solar Azimuth Angle (deg)*	*Albedo (Pyranometer) (%)*	*Albedo (Numerical Integration) (%)*	*Relative Δ (%)*	*Albedo (Walthall Model) (%)*	*Relative Δ (%)*
05/12/88	1012	43	107	23.82	23.44	−1.60	23.62	−0.84
(sod)	1035	39	112	23.13	22.94	−0.82	23.10	−0.13
	1104	34	120	22.36	22.12	−1.07	22.26	−0.45
	1135	29	130	21.69	21.59	−0.46	21.69	−0.00
	1204	25	143	21.22	21.05	−0.80	21.14	−0.39
	1232	22	158	21.00	20.51	−2.33	20.56	−2.10
	1306	21	182	20.62	20.37	−1.21	20.43	−0.92
	1334	22	199	20.70	20.21	−2.37	20.26	−2.13
	1408	25	218	21.06	20.45	−2.90	20.52	−2.56
	1429	28	227	21.08	20.79	−1.38	20.86	−1.02
	1503	33	239	21.78	21.24	−2.48	21.37	−1.88
	1534	39	248	22.61	22.23	−1.68	22.37	−1.06
	1603	44	255	23.45	23.11	−1.45	23.26	−0.81
	1637	50	261	24.62	24.14	−1.95	24.35	−1.10
	1703	55	266	25.84	25.13	−2.75	25.42	−1.63
	1738	62	272	27.39	27.21	−0.66	27.54	0.55
	1803	67	275	28.69	27.93	−2.65	28.40	−1.00
	1833	73	280	30.43	29.26	−3.84	29.86	−1.87
06/29/89	1631	45	265	17.37	17.25	−0.69	17.28	−0.52
(soil)	1709	52	271	17.37	17.57	1.15	17.65	1.61
	1834	68	283	17.82	18.37	3.09	18.73	5.11
	1911	75	288	18.23	18.43	1.10	18.90	3.68
06/30/89	0916	52	90	17.37	17.67	1.73	17.69	1.84
(soil)	0950	46	95	17.18	17.48	1.75	17.43	1.46
	1046	35	106	17.11	17.53	2.45	17.42	1.81
	1142	25	123	16.87	17.55	4.03	17.48	3.62
	1428	23	231	17.02	17.45	2.53	17.44	2.47
	1526	32	251	17.16	17.54	2.21	17.54	2.21
	1615	42	262	17.32	17.29	−0.17	17.34	0.12
	1647	48	267	17.28	17.14	−0.81	17.25	−0.17
	1656	49	268	17.48	17.10	−2.17	17.22	−1.49

Table 4. Intercept (b_0), Slope (b_1), Correlation Coefficients (r^2), and Root Mean Square Errors (rmse) for Comparisons of Albedo Estimated with Numerical Integration or Walthall Model and Albedo Measured with Pyranometers

	Numerical Integration					*Walthall Model*				
	b_0	b_1	r^2	*rmse (a) (%)*[a]	*rmse (r)*[a]	b_0	b_1	r^2	*rmse (a) (%)*	*rmse (r)*
Combined	1.706[b]	0.911[c]	0.994	0.449	2.050	1.208[b]	0.941[c]	0.993	0.366	1.884
Sod	0.867[b]	0.945[c]	0.994	0.502	2.010	−0.149	0.995	0.993	0.313	1.342
Soil	3.675	0.801	0.474	0.363	2.104	−3.996	1.247	0.659	0.428	2.440

$$\text{rmse}(a) = \left[\frac{1}{n}\sum_{i=1}^{n}(\varepsilon_i - \mathbf{p}_i)^2\right]^{1/2}, \qquad \text{rmse}(r) = 100\cdot\left[\frac{1}{n}\sum_{i=1}^{n}((\varepsilon_i - \mathbf{p}_i)/\mathbf{p}_i)^2\right]^{1/2},$$

where n is the number of observations, ε_i is the estimated albedo, and $\mathbf{p}_i$ is albedo measured with pyranometers.

[b] b_0 significantly different from 0.0 at $\alpha = 0.05$.

[c] b_1 significantly different from 1.0 at $\alpha = 0.05$.

were found to be statistically different from 0.0 and 1.0, respectively. rmse(a) and rmse(r) values for the numerical integration techniques were 0.5% and 2.0% for the combined data. rmse values from the Walthall model were slightly lower at 0.4% absolute errors and 1.9% relative errors.

SUMMARY

The results of this study support the use of discrete wavelength, multiple angle surface bidirectional reflectance factors data to estimate total shortwave albedo. Both numerical integration and integration of an empirical model fit to the data produced estimates of shortwave albedo that closely agreed with coincident independent measurements of albedo obtained by the more conventional use of pyranometers. The results of our analysis, based on a grass canopy and a tilled bare soil surface, also suggest that either albedo estimation technique may be used to characterize the hemispherical reflectance of surfaces with very different observed reflectance factor distributions (e.g., Plate IV).

Although albedos have been estimated from multiple direction reflectance factor data in the past, previous studies did not generally compare such estimates to independent albedo measurements. The close agreement found in this study between albedo estimated from reflectance factors and albedo from pyranometers validates the current and past use of multiple direction reflectance factor data to estimate albedo for similar surfaces. Additional studies of other surface types are needed to characterize the variability of albedo as a function of surface type and solar zenith angle.

The results of this study indicate that multiangle observations from new and future remote sensing instruments may be a viable approach for the characterization of terrestrial surface albedos. Pointable imaging spectroradiometers such as the airborne Advanced Solid-State Array Spectroradiometer (ASAS) (Irons et al., 1991) currently provide the capability to rapidly acquire multiple angle spectral data over a wide variety of terrestrial surfaces. Its capabilities can be explored using ground-based data similar to that employed in this study with appropriate treatment of atmospheric effects. The same is true for sensors proposed for the future Earth Observing System, for example, which are being designed to provide observations over the entire shortwave region from multiple view directions. These proposed sensors include the Moderate Resolution Imaging Spectrometer-Tilt (MODIS-T) (Salomonson et al., 1989), the High Resolution Imaging Spectrometer (HIRIS) (Goetz and Herring, 1989), and the Multiangle Imaging Spectroradiometer (MISR) (Diner et al., 1989).

These types of sensors will provide data from fewer view directions than the number of view directions utilized in this study. Further analyses of the available surface observations are needed to specify the minimum number and location of view directions required for accurate estimation of surface albedos.

Data on diurnal and seasonal albedo dynamics of many additional surface types are required to evaluate the expression of surface albedo in models of biophysical processes. In addition, global scale monitoring of surface albedos with stated accuracies of 2–15% (e.g., Way and Schier, 1989) are needed to detect environmental and climatic changes and to anticipate future changes. Although the techniques discussed here have been shown to estimate albedo within 3%, additional work is required to examine their validity under varying atmospheric and topographic conditions. Further efforts to establish remote sensing methods for determining surface albedo are well justified, since remote sensing offers the only practical means for repeatedly observing the albedo of diverse terrestrial surfaces on a global scale.

This work was funded by NASA Headquarters and Goddard Space Flight Center, Biospheric Sciences Branch. The authors wish to acknowledge the assistance of Frank Wood, Ned Horning, and Mike Bur in carrying out the measurements and Robert Katz for graphics support.

REFERENCES

Dickinson, R. E. (1983), Land surface processes and climate–surface albedos and energy balance, *Adv. Geophys.* 25:305–353.

Diner, D. J., Bruegge, C. J., Martonchik, J. V., Ackerman, T.P., Davies, R., Gerstl, S. A. W., Gordon, H. R., Sellers, P. J., Clark, J., Daniels, J. A., Danielson, E. D., Duval, V. G., Klaasen, K. P., Lilienthal, G. W., Nakamoto, D. I., Pagano, R. J., and Reilly, T. H. (1989), MISR: a multiangle imaging spectroradiometer for geophysical and climatological research from EOS, *IEEE Trans. Geosci. Remote Sens.* 27:200–214.

Goetz, A. F. H., and Herring, M. (1989), The High Resolution Imaging Spectrometer (HIRIS) for EOS, *IEEE Trans. Geosci. Remote Sens.* 27:136–144.

Idso, S. B., Hatfield, J. L., Reginato, R. J., and Jackson, R. D. (1978), Wheat yield estimation by albedo measurement, *Remote Sens. Environ.* 7:273–276.

Irons, J. R., and Smith, J. A. (1990), Soil surface roughness characterization from light scattering observations, in *Proc. IGARSS '90*, College Park, MD, 20–24 May, pp. 1007–1010.

Irons, J. R., Johnson, B. L., Jr., and Linebaugh, G. H. (1987), Multiple-angle observations of reflectance anisotropy from an airborne linear array sensor, *IEEE Trans. Geosci. Remote Sens.* GE-25:372–383.

Irons, J. R., Ranson, K. J., and Daughtry, C. S. T. (1988), Estimating big bluestem albedo from directional reflectance measurements, *Remote Sens. Environ.* 25:185–199.

Irons, J. R., Ranson, K. J., Williams, D. L., Irish, R. I., and Huegel, F. G. (1991), An off-nadir-pointing imaging spectroradiometer for terrestrial ecosystem studies, *IEEE Trans. Geosci. Remote Sens.* GE-29:66–74.

Jackson, R. D. (1984), Total reflected solar radiation calculated from multi-band sensor data, *Agric. For. Meteorol.* 33:163–175.

Kimes, D. S. (1983), Dynamics of directional reflectance factor distributions for vegetation canopies, *Appl. Opt.* 22:1364–1372.

Kimes, D. S., and Sellers, P. J. (1985), Inferring hemispherical reflectance of the earth's surface for global energy budgets from remotely sensed nadir of directional radiance values, *Remote Sens. Environ.* 18:205–223.

Kimes, D. S., Sellers, P. J., and Newcomb, W. W. (1987), Hemispherical reflectance variations of vegetation canopies and implications for global and regional energy budget studies, *J. Climate Appl. Meteorol.* 26:959–972.

Kneizys, F. X., Shettle, E. P., Gallery, W. O., Chetwynd, J. H., Jr., Abeau, L. W., Selby, J. E. A., Clough, S. A., and Fenn, R. W. (1983), Atmospheric transmittance/radiance: computer code LOWTRAN 6, Environmental Research Papers, No. 846, Optical Physics Division, Air Force Geophysics Laboratory, Hanscom AFB, MA.

Kriebel, K. T. (1979), Albedo of vegetated surfaces: its variability with differing irradiances, *Remote Sens. Environ.* 8:283–290.

Pinker, R. T., and Ewing, J. A. (1986), Effect of surface properties on the narrow to broadband spectral relationship in clear sky satellite observations, *Remote Sens. Environ.* 20:267–282.

Pinker, R. T., and Stowe, L. L. (1990), Modelling planetary bidirectional reflectance over land, *Int. J. Remote Sens.* 11:113–123.

Robinson, B. F., and Biehl, L. L. (1979), Calibration procedures for measurement of reflectance factor in remote sensing field research, in *Proceedings of the Society of Photo-Optical Instrumentation Engineering, 23rd Annual Technical Symposium on Measurements of Optical Radiation*, SPIE, Bellingham, WA, pp. 16–26.

Salomonson, V. V., Barnes, W. L., Maymon, P. W., Montgomery, H. E., and Ostrow, H. (1989), MODIS: advanced facility instrument for studies of the earth as a system, *IEEE Trans. Geosci. Remote Sens.* 27:145–153.

Saunders, R. W. (1990), The determination of broad band surface albedo from AVHRR visible and near-infrared radiances, *Int. J. Remote Sens.* 11:49–67.

Seller, P. J. (1985), Canopy reflectance, photosynthesis and transpiration, *Int. J. Remote Sens.* 6:1335–1372.

Walthall, C. L., Norman, J. M., Welles, J. M., Campbell, G., and Blad, B. L. (1985), Simple equation to approximate the bidirectional reflectance from vegetative canopies and bare soil surfaces, *Appl. Opt.* 24:383–387.

Way, J. B., and Schier, M. (1989), EOS interdisciplinary scientists' silver bullets and data product input/output, Vol. 2, Version 1.1, Jet Propulsion Laboratory, 4800 Oak Grove Drive, Pasadena, CA 91109.

Wiesnet, D. R., and Matson, M. (1983), Remote sensing of weather and climate, in *Manual of Remote Sensing*, 2nd ed. (J. E. Estes and G. A. Thorley, Eds.), American Society of Photogrammetry, Falls Church, VA, Vol. II.